International Journal of Biological Macromolecules 124 (2019) 1299–1311

Contents lists available at ScienceDirect

International Journal of Biological Macromolecules

journal homepage: http://www.elsevier.com/locate/ijbiomac

Co-delivery of 5-fluorouracil and oxaliplatin in novel poly (3-hydroxybutyrate-*co*-3-hydroxyvalerate acid)/poly (lactic-*co*-glycolic acid) nanoparticles for colon cancer therapy

Somayeh Handali [a], Eskandar Moghimipour [a,b], Mohsen Rezaei [c], Sadegh Saremy [b], Farid Abedin Dorkoosh [d,e,*]

[a] Nanotechnology Research Center, Ahvaz Jundishapur University of Medical Sciences, Ahvaz, Iran
[b] Cellular and Molecular Research Center, Ahvaz Jundishapur University of Medical Sciences, Ahvaz, Iran
[c] Department of Toxicology, Faculty of Medical Sciences, Tarbiat Modares University, Tehran, Iran
[d] Department of Pharmaceutics, Faculty of Pharmacy, Tehran University of Medical Sciences, Tehran, Iran
[e] Medical Biomaterial Research Centre (MBRC), Tehran University of Medical Sciences, Tehran, Iran

ARTICLE INFO

Article history:
Received 17 May 2018
Received in revised form 12 September 2018
Accepted 20 September 2018
Available online 21 September 2018

Keywords:
5-Fluorouracil
Oxaliplatin
Cancer
Poly(3-hydroxybutyrate-*co*-3-hydroxyvalerate acid)
Poly(lactic-*co*-glycolic acid)
ROS
Apoptosis

ABSTRACT

In the present study, a novel 5FU and OXA co-loaded PHBV/PLGA NPs was developed which induced apoptosis in cancer cells. NPs were prepared by the double emulsion method and their preparation was optimized using D-optimal design of response surface methodology (RSM). 5FU-OXA loaded NPs were evaluated by SEM, DSC and DLS. NPs were spherical as shown by SEM and the results of DSC indicated that both drugs successfully entrapped into NPs. 5FU-OXA loaded NPs exhibited higher cytotoxicity effect than free drugs on cancer cells. For the first time to our knowledge, these results showed that more ROS generation and stronger activation of the ROS-dependent apoptotic pathway were induced by 5FU and OXA delivered by NPs. Furthermore, it was observed that NPs were hemocompatible. Co-loaded NPs exhibited significantly higher antitumor efficiency compared to free drugs combination, indicating this co-delivery system provides great potential in cancer therapy. The results of present study also confirmed that PHBV/PLGA NPs can be served as a promising platform for the co-delivery of antitumor drugs and present a new view for treatment of cancer with reducing side effect of drugs.

1. Introduction

5-Fluorouracil (5FU) is a first-line chemotherapeutic agent for treatment of colon cancer. It is a pyrimidine analog which interferes with thymidylate synthesis [1,2]. However, its medical application is limited due to poor membrane permeability, short half-life (5–20 min), wide distribution to healthy tissues and severe side effects including gastrointestinal, hematological, cardiac toxicities, hair loss, liver disease, birth defects, mouth sores and ulcers [1,3–6]. Moreover, it has been reported that the lower cytotoxicity of 5FU may be associated to the drug resistance due to efflux of 5FU by P-glycoprotein (P-gp) pumps [7]. 5FU is usually administrated in combination with some other drugs to achieve more effectiveness [8].

At present oxaliplatin (OXA) is extensively used along with 5FU for the treatment of colon cancer [9]. OXA is a third generation platinum drug which inhibits DNA replication. Nevertheless, it still exhibit great adverse effects such as acute dysthesias, myelosupression, peripheral distal neurotoxicity, hematological and gastrointestinal toxicity [10–13].

Employing of nanoparticle (NPs) as drug delivery systems provide a platform for co-delivering of drugs with enhancing the anticancer efficacy, reducing side effects, increasing the circulation half-life of drugs, improving the distribution of drugs and overcoming drug resistance [13,14]. Moreover, NPs can deliver the high doses of drugs into cancer cells while bypass normal cells [14]. A number of NPs have been studied as drug delivery systems for improving the treatment of cancer including nanostructure lipid carrier (NLC), liposomes, polymeric NPs, dendrimers, cyclodextrin, gold nanoshells, carbon nanotubes and solid lipid nanoparticle (SLN) [15–19]. Recently, polymeric NPs have gained more consideration due to their biodegradability, biocompatibility, physical and chemical stability, protection of drugs against enzymatic degradation, ability to entrapment a variety of therapeutic agents and capability to conjugate [20–22]. For example polyhydroxyalkanoates (PHA) exhibit sufficient mechanical strength to make them suitable

Abbreviations: 5FU, 5-Fluorouracil; OXA, Oxaliplatin; PHBV, Poly(3-hydroxybutyrate-*co*-3-hydroxyvalerate); PLGA, Poly(lactic-*co*-glycolic acid); ROS, Reactive Oxygen Species; DAPI, Paraformaldehyde and 4,6-diamidino-2-phenylindole; MTT, 3-(4,5-dimethyl-2-thiazolyl)-2,5-diphenyl tetrazolium bromide; DMEM, Dulbecco's modified eagle's medium; DCF, Dichlorodihydrofluorescein; DCFDA, 2′,7′-dichlorofluorescin diacetate; FBS, Fetal bovine serum; DSC, Differential scanning calorimeter; SEM, Scanning electron microscopy.

* Corresponding author at: Department of Pharmaceutics, Faculty of Pharmacy, Tehran University of Medical Sciences, Tehran 14399-56131, Iran.
E-mail address: dorkoosh@tums.ac.ir (F.A. Dorkoosh).

https://doi.org/10.1016/j.ijbiomac.2018.09.119
0141-8130/

for treatment of muscle-fascial wounds. Also, due to high biocompatibility, PHA is an ideal candidate for production of scaffolds, which can be used to repair damage in various types of tissue [23,24].

Poly(3-hydroxybutyrate-*co*-3-hydroxyvalerate) is a natural polymer that is synthesized by bacteria. It has been studied extensively as a polymer for tissue engineering and as drug delivery systems. The polymer is biocompatible, biodegradable, and nontoxic [25,26]. PHBV unlike poly (lactic-*co*-glycolic acid) (PLGA), does not produce acidic degradation products which may be damaging for human tissues [27,28]. In addition, in comparison with PLGA, PHBV is economical with a low production cost [20]. However, low entrapment of hydrophilic molecules is one of the main disadvantages using of PHBV. On the other hand, it has been reported that PLGA NPs have high ability for entrapment of drugs [29]. PLGA is a synthetic copolymer which is widely employed as drug delivery system for improving anticancer activity of drugs owing to its biodegradable, biocompatible, non-immunogenic and non-toxic [30]. Nair et al. found that 5FU loaded PLGA NPs exhibited more antitumor activity with lower dose than free 5FU [1]. Lin et al. reported that 5FU loaded PLGA microsphere enhanced the drug concentration in the cancer cells more than free drug and decreased the toxicity of 5FU in the healthy cells [31]. Moreover, JQ et al. showed that OXA encapsulated PLGA microspheres significantly inhibited tumor growth and no significant adverse effects were observed on the mice during treatment [32].

In the present study for protecting the good biocompatibility of PHBV and improving the encapsulation efficiency, a novel PHBV/PLGA NPs is introduced as a platform for co-delivery of 5FU and OXA.

2. Materials and method

5-Fluorouracil (5FU) and oxaliplatin (OXA) were purchased from Acros, USA and Afine Chemical, China, respectively. Poly (3-hydroxybutyrate-*co*-3-hydroxyvalerate) (PHBV (molecular weight 4117.8 Da), containing 2–3% 3-hydroxyvalerate (3HV) by weight was acquired from Tianan Biologic Materials Ltd., Hangzhou, China. Poly(lactic-*co*-glycolic acid) (PLGA, 50:50, molecular weight 30,000–60,000), polyvinyl alcohol (PVA, average molecular weight 30,000–70,000), 5 (6)-carboxyfluorescein (CF), paraformaldehyde and 4,6-diamidino-2-phenylindole (DAPI) were obtained from Sigma-Aldrich, Germany.

HT-29 (human colorectal adenocarcinoma) and CT26 (murine colon carcinoma) were acquired from Iranian Biological Resource Center (IBRC) and National Cell Bank of Iran (NCBI), Pastor Institute of Iran, respectively. 3-(4,5-dimethyl-2-thiazolyl)-2, 5-diphenyl tetrazolium bromide (MTT) and 2′,7′-dichlorofluorescin diacetate (DCFDA) were acquired from Sigma-Aldrich, Germany. Dulbecco's modified eagle's medium (DMEM) and fetal bovine serum (FBS) were obtained from Gibco, USA. Penicillin-streptomycin was purchased from Sigma-Aldrich, Germany. Male BALB/c mice and male Wistar rats were obtained from the Pasteur Institute of Iran. Other chemicals and solvents were of analytical grade and purchased from Merck, Germany.

2.1. Experimental design

In the current study, 16 formulations with 2 independent variables including PHBV/PLGA ratio (X_1) and PVA concentration (X_2) were assessed using D-optimal design of response surface methodology (RSM). D-optimal design, as a technique is a design for 1 to 30 factors that minimizes the variance associated with the coefficient estimates for model. This technique assists the selection of the model which can precisely and accurately define parameter–response relationship. D-optimal design is suitable to investigate the least number of experiments to perform, analyze the effects that changes in mixture composition produce and help in the selection of the optimal composition for achieving the optimized formulation [33].

The dependent variables included the encapsulation efficiency (EE%) of 5FU (Y_1), EE% of OXA (Y_2) and particle size (PZ) (Y_3) of NPs.

Table 1
Variables and their levels used in D-optimal design.

Independent variables	Factors	Units	Levels	
			Low	High
X_1	PHBV/PLGA ratio	–	1	3
X_2	PVA	%	0.25	2

Dependent variables	Units	Constrains
Y_1: EE% (5FU)	%	Maximum
Y_2: EE% (OXA)	%	Maximum
Y_3: Particle size	nm	Minimum

Experimental factors and their levels were determined in preliminary studies. The variables and their levels are shown in Table 1. Design-Expert® software (version 7.0.0, stat-Ease, Inc., Minneapolis, MN) was employed for assessment of the data of the experiment. In order to determine the relationship and interaction between the variables and responses, the 3D response surfaces were also generated. Significance of the variables on the responses and the model was evaluated by ANOVA test (p-value < 0.05). The adequacy of the model was assessed by the correlation coefficients (R^2) and adjusted R^2. The optimized predicted formulation was prepared and the responses were compared with the predicted values.

2.2. Preparation of 5FU-OXA loaded PHBV/PLGA NPs

5FU-OXA loaded PHBV/PLGA NPs were prepared by the double emulsion ($W_1/O/W_2$) method. Briefly, 5FU (3 mg/mL) and OXA (2 mg/mL) were added drop wise into polymers solution dissolved in chloroform that consisted of PHBV and PLGA in different ratios as described in the Table 1 (polymer concentration: 2.5% w/v) followed by homogenizer at 20,000 rpm (Heidolph, Germany) for 5 min leading to the preparation of primary emulsion (W_1/O). In the next step, the resulting solution was drop wise added to an aqueous phase (W_2) containing PVA as an emulsifier (in different concentrations), which was homogenized again. The emulsion was stirred at room temperature to evaporate the organic solvent. Then, resulting suspension was centrifuged at 15,000 rpm for 30 min (MPW-350R, Poland) and the pellet was washed with distilled water and finally lyophilized at −50 °C (2 Pa) for 24 h (Operon, Korea) for further studies. The schematics preparation of NPs is shown in Fig. 1.

2.3. Determination of encapsulation efficacy

After centrifugation the concentration of free drugs in the supernatant was determined by high performance liquid chromatography (HPLC, Waters, USA) with the following conditions: C_{18} column (250 × 4 mm i.d., 5 μm); mobile phase: 0.02 M phosphate buffer (pH 4) and methanol (90:10, V/V); flow rate of 0.8 mL/min; detection wavelength: 260 nm; column temperature: 30 °C and injection volume: 50 μL. The drugs EE% was calculated using Eq. (1):

$$EE\% = (A-B/A) \times 100 \quad (1)$$

where A is the initial amount of drug added and B is the amount of remained free 5FU in supernatant after centrifugation determined by HPLC [34].

2.4. Morphological study and particle size determination

The morphology of NPs was examined by field emission scanning electron microscopy (FESEM, S4160, and Hitachi, Japan). The samples were prepared by evaporating a drop of NPs solution on carbon coated copper grid. The particle size of NPs was also determined by particle sizer (Qudix, ScatterOScope I, Korea) system at 25 °C. Before the measurement, the NPs suspension were diluted in deionised water and

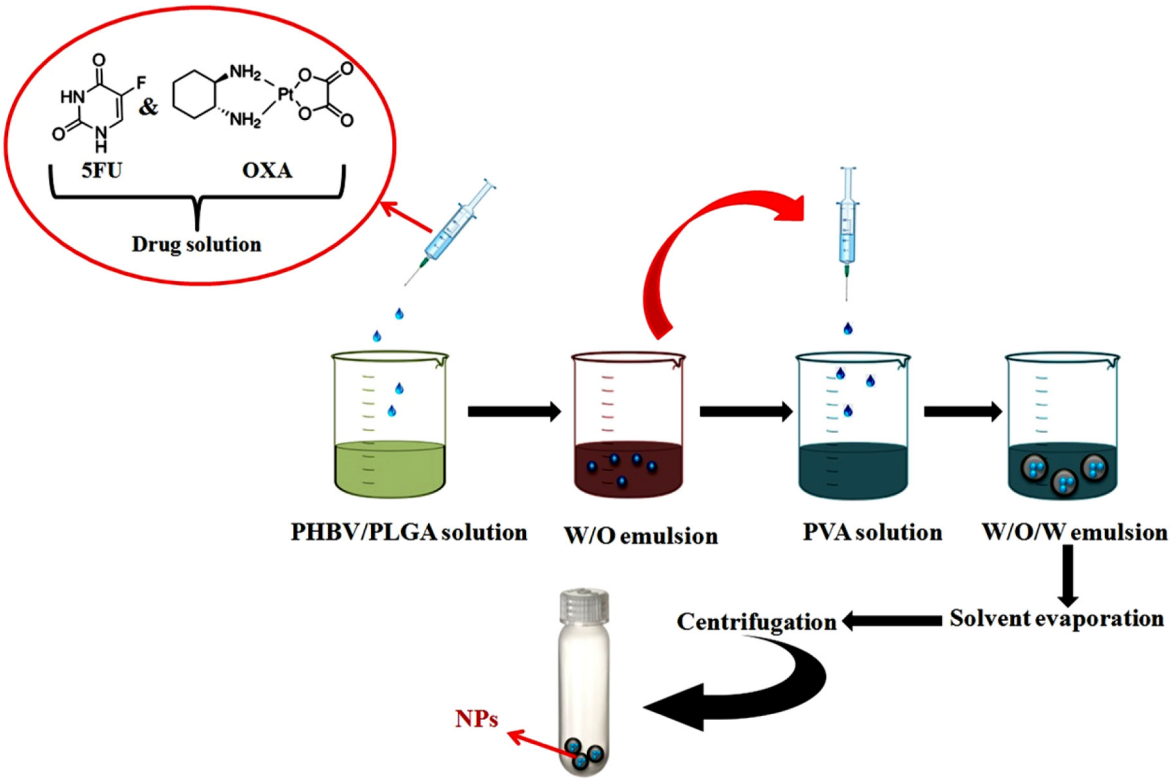

Fig. 1. Schematic preparation of 5FU-OXA loaded PHBV/PLGA NPs.

sonicated in ultrasonic bath (Elma, Germany) for preventing particles agglomeration.

2.5. DSC analysis

DSC studies were performed to evaluate physical state of 5FU and OXA in the NPs [35]. Thermal behavior of PHBV, PLGA, 5FU, OXA and 5FU-OXA loaded PHBV/PLGA NPs were performed using a differential scanning calorimeter (DSC-1 Mettler Toledo, Switzerland). 5 mg of each sample were sealed in aluminum pans and a heating rate of 10 °C/min was employed in the 0 to 300 °C temperature range.

2.6. In vitro release

In vitro release of drugs from the NPs was determined by the dialysis bag method. Briefly, about 1 mL of the NPs formulation and free drugs were tightly sealed in a dialysis bag (MW cut off 12 kDa) and immersed in dialysis medium. At predetermined time intervals, 500 μL of the medium was taken for analysis and fresh medium of an equal volume was replaced. The amount of drugs in the receptor phase was assayed using HPLC method.

2.7. In vitro cellular uptake of NPs

Because 5FU and OXA are non-fluorescent drugs, CF loaded PHBV/PLGA NPs were prepared for evaluation of the cellular uptake of NPs. HT-29 cells were seeded on 6-well plates at a density of 1×10^5 cells/well. After 24 h, the culture medium was replaced with growth medium containing free CF and CF loaded PHBV/PLGA NPs and incubated for 4 and 24 h at 37 °C. Then, the cells were washed with PBS and fixed in 4% paraformaldehyde for 15 min at room temperature. Then, the cells were stained with 4,6-diamidino-2-phenylindole (DAPI) for 10 min. The internalized CF was observed using fluorescent microscope (Olympus IX71, Japan).

2.8. Cell viability assay

The in vitro cytotoxicity of free 5FU and OXA and 5FU-OXA loaded PHBV/PLGA NPs were evaluated by MTT assay. HT-29 and CT26 cells were cultured in DMEM supplemented with 10% FBS and 1% penicillin-streptomycin and incubated overnight at 37 °C. The cells were seeded in a 96-well plate at density of 1×10^4 cells/well and allowed to attach and grow for 24 h. Then, the cells were treated with different concentrations of free 5FU and OXA and 5FU-OXA loaded PHBV/PLGA NPs for 48 h. 20 μL of MTT (5 mg/mL) was added in each well and incubated for 4 h. Afterward, 100 μL of DMSO was added to each well in order to dissolve the formazan crystals and the plates were gently shaken for 20 min. The absorbance was recorded at 570 nm using ELISA plate reader (BioRad, USA) and survival rates were calculated by following equation:

$$\text{Cell viability}\% = (\text{Abs}_{\text{sample}}/\text{Abs}_{\text{control}}) \times 100 \quad (2)$$

where $\text{Abs}_{\text{sample}}$ is related to the absorbance of cells treated with mixture of free 5FU and OXA or the drugs loaded NPs and $\text{Abs}_{\text{control}}$ is attributed to the absorbance of cells without any drug treatment. According to the cell viability values, IC_{50} (inhibitory concentration to produce 50% cell death) was also calculated.

2.9. Reactive oxygen species (ROS) detection

2′,7′-Dichlorofluorescin diacetate (DCFDA) was used for determination of ROS generation in cells. DCFDA, a non-fluorescent probe can penetrate into the cells and then oxidize by intracellular ROS to fluorescent dichlorodihydrofluorescein (DCF) [36]. Briefly, the cells were seeded into 6-well plates at a density of 2×10^5 cells/well and incubated for 24 h. After incubation, the cells were treated with IC_{50} dose of free 5FU and OXA and 5FU-OXA loaded PHBV/PLGA NPs for 2, 24 and 48 h. After treatment, the medium was removed and 10 μM of DCFDA was added to the cells. The cells were then kept in the incubator for

45 min. Fluorescence was monitored at excitation wavelength of 485 nm and emission wavelength of 530 nm using spectrofluorimeter (PerkinElmer, USA).

2.10. Apoptosis study

DAPI forms fluorescent complexes with natural double-stranded DNA and is helpful to detect the apoptotic nuclei [37]. Therefore, in the study, DAPI staining was used to determine apoptosis by fluorescence microscopy. Briefly, HT-29 cells were cultured in 6-well plates and treated with IC_{50} dose of free 5FU and OXA and 5FU-OXA loaded NPs for 48 h. After treatment, the grown medium was removed and cells were washed with PBS and permeabilized in 0.1% Triton X-100 for 10 min. Then, the cells were fixed with 4% paraformaldehyde, washed again with PBS and stained with DAPI (2 mg/mL) for 10 min at room temperature. Medium without formulation was also considered as control. Apoptotic cells were evaluated using fluorescent microscope (Olympus IX71, Japan). Apoptotic cells were recognized by nuclear condensation and fragmentation [4].

2.11. Hemolysis assay

The hemolytic potentials of NPs were evaluated in vitro using the red blood cells (RBCs). Fresh blood of Wistar rats was collected and RBCs were separated by centrifugation at 1500 rpm/min for 10 min. Then, the RBCs were washed three times using PBS. 900 μL of PHBV/PLGA NPs at different concentrations (0.01, 0.05, 0.1, 0.25, 0.5 and 1 mg/mL) were added to 900 μL of RBCs suspension and incubated for 3 h at 37 °C. Then, unlysed erythrocytes were separated by centrifugation at 1500 rpm for 10 min, the supernatant was collected and the optical density (OD) of the supernatant was read in a spectrophotometer (Biochrom WPA biowave II, England) at 540 nm. Triton X-100 (10%) and PBS were used as positive and negative controls, respectively. The hemolysis (%) was determined by following formula:

$$\text{Hemolysis}\ (\%) : \left(A_s - A_{nc} / A_{pc} - A_{nc}\right) \times 100 \quad (3)$$

where, A_s is the absorbance of sample, A_{nc} is the absorbance of negative control and A_{pc} is the absorbance of positive control.

2.12. In vivo antitumor activity and histopathological study

All animal experiments were carried out following the protocol approved by the Animal Ethics Committee Jundishapur University of Medical Sciences, Ahvaz, Iran (ref no. IR.AJUMS.REC.1395.643). The mice were subcutaneously injected with 0.1 mL of cell suspension containing 1×10^6 CT26 cells. When the average volume of the tumors reached to 100 mm^3, the mice were randomly divided into the following three groups: 1) control, 2) 5FU and OXA and 3) 5FU-OXA loaded PHBV/PLGA NPs. Formulations were injected via intraperitoneally on days 6, 9, 12 after inoculation. The dosage of 5FU and OXA were selected as 25 and 5 mg/kg, respectively according to the literature [38,39]. The average volume of tumors was calculated using following formula:

$$V = \left(W^2 \times L\right)/2 \quad (4)$$

where W is the shortest diameter and L is the longest diameter.

At the end of treatment, the mice were sacrificed and tumors were excised, fixed with 10% paraformaldehyde. Then, the tumors were embedded in paraffin, sectioned and stained with hematoxylin and eosin (H&E) and observed using optical microscope (Olympus BX53P, Japan).

2.13. Statistical analysis

All the data were presented as mean ± SD and statistical analysis was performed using one-way ANOVA. Differences were considered statistically significant at a p value < 0.05.

3. Results and discussion

3.1. Experimental design

RSM is less time-consuming than other approaches due to small number of experimental runs are requirement for monitoring the interaction between independent and dependent variables [40]. In this study, D-optimal design was employed for the optimization of NPs. This design provides an experimental model to determine the effect of formulation components on the loading of drugs and particle size of

Table 2
D-optimal design in various runs and correspondent responses.

Run	PHBV/PLGA ratio	PVA (%)	EE% (5FU)	EE% (OXA)	PZ (nm)
1	1.88	2.00	51.2347	35.299	245
2	3.00	2.00	55.9507	38.43	329
3	3.00	1.13	56.0529	29.8671	110
4	2.13	1.24	55.823	32.78	79.8
5	3.00	0.25	35.831	26.0769	159
6	1.00	0.25	39.542	1.043	80.2
7	1.00	0.25	39.4694	12.87	86.9
8	3.00	0.25	36.3204	25.54	155
9	3.00	2.00	55.5679	38.521	320
10	2.31	0.39	37.0749	19.01	61.8
11	1.00	2.00	52.3274	25.2587	148
12	1.60	0.25	41.0999	4.098	64.8
13	1.00	0.78	16.23	12.09	75.2
14	1.00	2.00	52.841	16.6923	146
15	1.16	1.40	46.0168	12.65	78.1
16	3.00	1.13	56.3985	30.8304	116

Table 3
The analysis of variances for EE% of 5FU as the response (Y_1).

Source	Sum of squares	df	Mean square	F value	p-Value*
Model	1877.09	9	208.57	2290.55	<0.0001
X_1	108.97	1	108.97	1196.71	<0.0001
X_2	420.01	1	420.01	4612.76	<0.0001
X_1X_2	23.00	1	23.00	252.57	<0.0001
X_1^2	20.48	1	20.48	224.92	<0.0001
X_2^2	16.62	1	16.62	182.52	<0.0001
$X_1^2X_2$	29.74	1	29.74	326.65	<0.0001
$X_1X_2^2$	344.97	1	344.97	3788.60	<0.0001
X_1^3	20.27	1	20.27	222.61	<0.0001
X_2^3	324.81	1	324.81	3567.15	<0.0001
Residual	0.55	6	0.091		
Lack of fit	0.16	1	0.16	2.05	0.2112
Pure error	0.39	5	0.077		
Cor total	1877.64	15			
R^2	0.9897				
Adjusted R^2	0.9993				

* Significant at 0.05 level.

Table 4
The analysis of variances for EE% of OXA as the response (Y_2).

Source	Sum of squares	df	Mean square	F value	p-Value*
Model	1781.20	2	890.60	39.24	<0.0001
X_1	1041.08	1	1041.08	45.87	<0.0001
X_2	714.22	1	714.22	31.47	<0.0001
Residual	295.05	13	22.70		
Lack of fit	187.80	8	23.48	1.09	0.4824
Pure error	107.24	5	21.45		
Cor total	2076.25	15			
R^2	0.8579				
Adjusted R^2	0.8360				

* Significant at 0.05 level.

Table 5
The analysis of variances for NPs size as the response (Y_3).

Source	Sum of squares	df	Mean square	F value	p-Value*
Model	1.110E+005	9	12,334.14	687.45	<0.0001
X_1	8.43	1	8.43	0.47	0.5186
X_2	645.60	1	645.60	35.98	0.0010
X_1X_2	5653.56	1	5653.56	315.10	<0.0001
X_1^2	1194.22	1	1194.22	66.56	0.0002
X_2^2	21,954.21	1	21,954.21	1223.63	<0.0001
$X_1^2X_2$	2549.93	1	2449.93	142.12	<0.0001
$X_1X_2^2$	3223.52	1	3223.52	179.66	<0.0001
X_1^3	165.50	1	165.50	9.22	0.0229
X_2^3	254.97	1	254.97	14.21	0.0093
Residual	107.65	6	17.94		
Lack of fit	16.71	1	16.71	0.92	0.3819
Pure error	90.95	5	18.19		
Cor total	1.111E+005	15			
R^2	0.9990				
Adjusted R^2	0.9976				

NPs [41]. The values of independent variables and responses in 16 suggested formulations based on D-optimal design are presented in Table 2.

The analysis of variance for EE% of 5FU as a response is displayed in Table 3. According to the results a cubic model was fitted as follows:

$$Y_1 = +132.57783 - 92.56640\,(X_1) - 258.93824\,(X_2) + 19.92998\,(X_1X_2) + 54.62049\,(X_1)^2 + 255.74289\,(X_2)^2 + 4.89564\,(X_1)^2\,(X_2) - 16.71095\,(X_1)\,(X_2)^2 - 10.49962\,(X_1)^3 - 64.93626\,(X_2)^3 \quad (5)$$

where Y_1 is the predicted EE% of 5FU and X_1 and X_2 are PHBV/PLGA ratio and PVA concentration, respectively. As depicted in the Table 3, the lack of fit of the model was found to be not significant ($F = 2.05$; p value = 0.2112). Non-significant lack of fit is good for a model to fit [42]. Also, the p-value of the model is below 0.05 which indicated that the model can significantly exhibit the real association between variables and response. The value of R^2 and adjusted R^2 of this model were 0.98 and 0.99, respectively, indicating a good fit between the response model and the experimental values.

Based on the results of Table 4, the liner model (Eq. (6)) is the best fitted model for EE% of OXA in NPs with F-value of 1.09 (p value = 0.4824).

$$Y_2 = -6.10333 + 9.31746\,(X_1) + 9.23534\,(X_2) \quad (6)$$

where Y_2 is the predicted EE% of OXA and X_1 and X_2 are PHBV/PLGA ratio and PVA concentration, respectively. The R^2 and adjusted R^2 of this model were predicted to be 0.85 and 0.83, respectively. The proximity between R^2 and adjusted R^2 indicated the efficiency of the model to predict EE% of OXA.

According to the results of Table 5, the cubic model is the best model proposed for particle size of NPs with the following equation:

$$Y_3 = +58.61970 + 92.84012\,(X_1) + 15.67278\,(X_2) + 96.37405\,(X_1X_2) - 107.10309\,(X_1)^2 - 181.45001\,(X_2)^2 - 45.32958\,(X_1)^2(X_2) + 51.08284\,(X_1)\,(X_2)^2 + 30.00195\,(X_1)^3 + 57.53382\,(X_2)^3 \quad (7)$$

where Y_3 is the particle size and X_1 and X_2 are PHBV/PLGA ratio and PVA concentration, respectively. Insignificant lack of fit ($F = 0.92$; p value = 0.3819) further confirms that the selected models adequately fit the data. The coefficient of determination (R^2) and adjusted R^2 of this model were predicted to be 0.99. The determination coefficient (R^2)

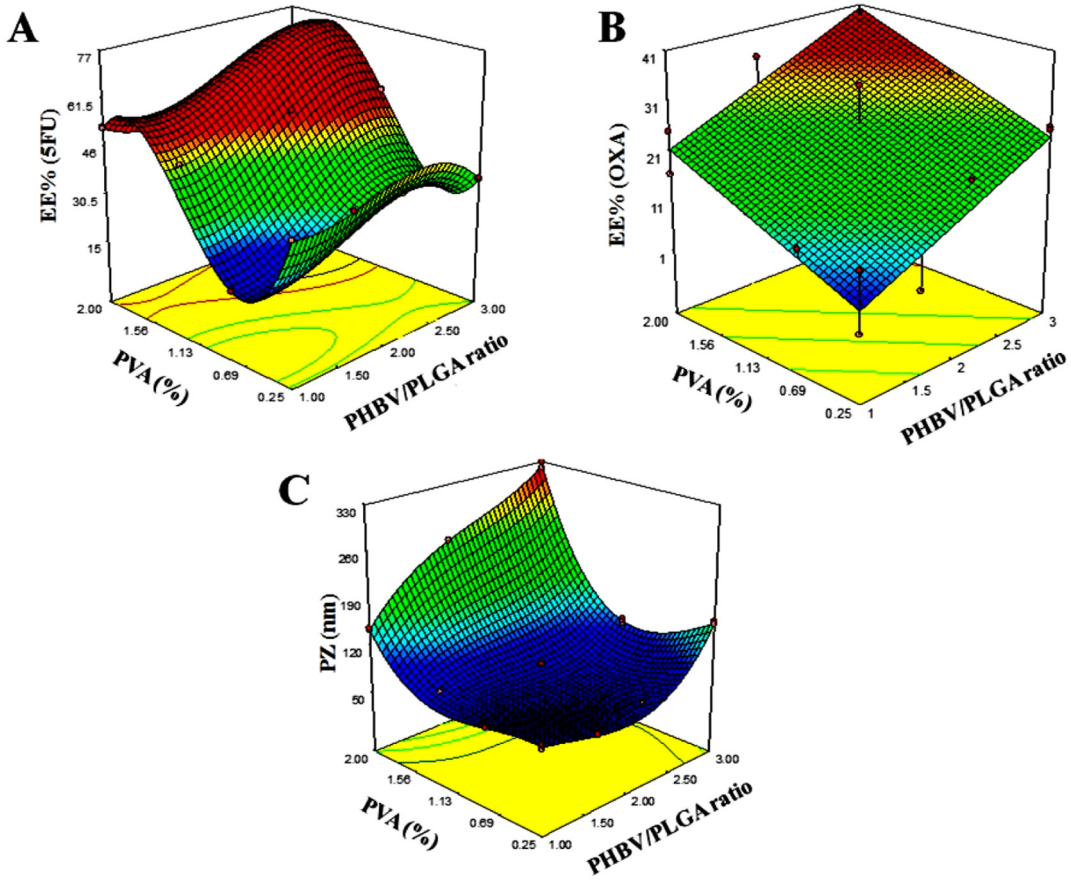

Fig. 2. Response surface plots for A) EE% of 5FU, B) EE% of OXA and C) particle size of NPs.

Table 6
Predicted and observed responses obtained at optimum conditions.

Independent variable		Optimized amount	Dependent variable		Predicted amount	Observed amount	Prediction error (%)
X_1	PHBV/PLGA ratio	2.75	Y_1	EE%	59.83	50.95	14.84
X_2	PVA	1.16	Y_2	EE%	30.24	26.31	12.99
			Y_3	PZ	90.62	92.8	2.40

demonstrated that 99.00% of the variability in the response could be explained by the model.

The 3D response surfaces plot was used to show the effect of interaction between variables on the EE% and size of NPs (Fig. 2). As displayed in Fig. 2A and C, EE% (5FU) and particle size do not show linear relationship with PHBV/PLGA ratio or PVA concentrations since they show cubic model (for example, EE% (5FU) increases with the increase of PVA% within certain range of the PVA% that show linear relationship, however, the EE% (5FU) drops at the higher end range of PVA% (~1.56 to 2).

According to Fig. 2B, EE% of OXA was enhanced by increasing the PHBV/PLGA ratio and PVA concentration.

3.2. Optimization and validation of the model

The optimized formulation was developed and characterized for maximum EE% of both drugs and the smallest particle size. Predicted and actual values of responses are shown in Table 6. As seen in Table 6, the observed amounts were in good agreement with the predicted values generated by the RSM which indicated significance and predictability of models. These findings also confirmed that the D-optimal design method can be successfully used for designing NPs.

3.3. Morphological study and particle size determination

The optimized NPs formulation was found to be spherical in shape with no particle aggregation (Fig. 3). Moreover, particle size analysis results showed that 5FU-OXA loaded PHBA/PLGA NPs were approximately 92.8 nm in size and exhibited a monodisperse distribution (Fig. 4). The nano-size of drug delivery systems is considered as an important feature that significantly affects the biodistribution of NPs as well as provides higher surface area and more accessibility inside the blood vessels of tumor tissue to reach better permeation [14,20]. According to the literature, NPs larger than 220 nm are generally taken up from the circulation by phagocytic cells; moreover, NPs smaller than 10 nm are fall down into renal filtration and urinary excretion [43]. Therefore, in order to internalize NPs into cells, their size should be small enough to get away from macrophages and large enough to avoid rapid renal filtration. According to previous studies, it seems that the mean size of NPs in the range of 10–220 nm is ideal. In our study, the resulted optimized NPs had particle sizes approximately 92.8 nm which has the mentioned advantaged simultaneously.

3.4. DSC analysis

DSC curves of 5FU, OXA, PHBV, PLGA and 5FU-OXA loaded PHBV/PLGA NPs are shown in Fig. 5. Free 5FU and OXA displayed sharp endothermic peaks at temperature of 282 °C and 300 °C, respectively which are in accordance with the literature values [44–47]. PHBV and PLGA

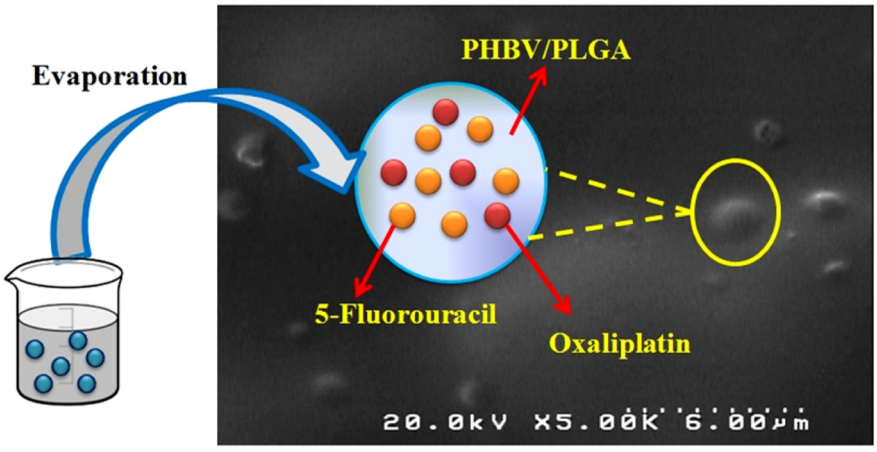

Fig. 3. SEM image of 5FU-OXA loaded PHBV/PLGA NPs.

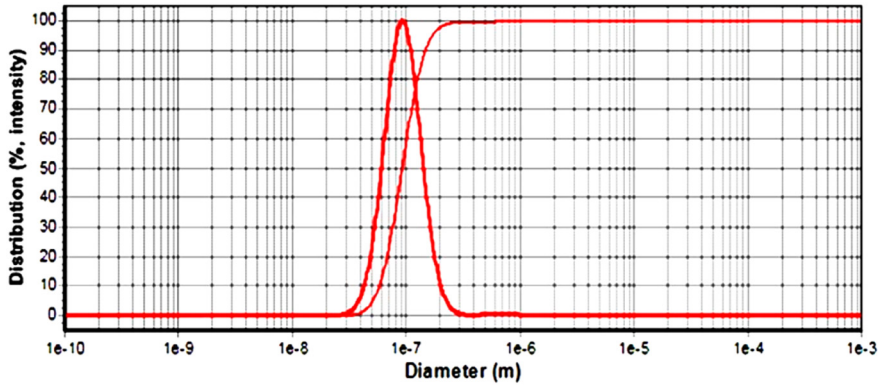

Fig. 4. Particle size distribution of 5FU-OXA loaded PHBV/PLGA NPs.

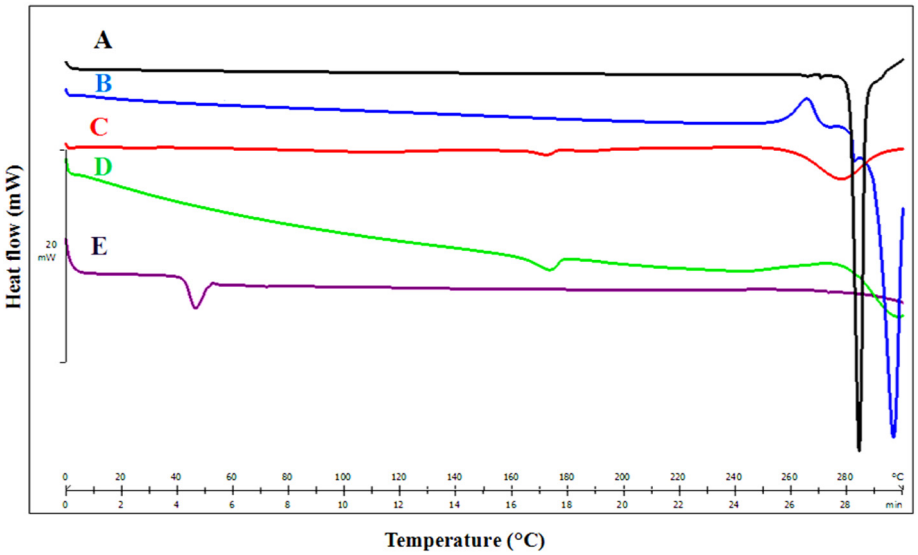

Fig. 5. DSC thermograms of A) 5FU, B) OXA, C) 5FU-OXA loaded PHBV/PLGA NPs, D) PHBV and E) PLGA.

polymer showed endothermic peaks at 177 °C and 48 °C, respectively, confirming previously reported data [48–50]. The typical melting peaks of 5FU and OXA were not observed in DSC curves of PHBV/PLGA NPs which indicates that conversion of both drugs from the crystalline state to the amorphous state. In addition, the absence of 5FU and OXA peaks can be associated to the entrapment of drugs in the NPs.

3.5. In vitro release

The release profile of free drugs and the optimized NPs formulation co-encapsulating 5FU and OXA are shown in Fig. 6. According to the results, free drugs were rapidly released within 4; however, the release rate of both drugs in the NPs was obviously slower than their solutions. Therefore, it can be concluded that encapsulated of the drugs in NPs can better control the release of the drugs.

3.6. In vitro cellular uptake of NPs

In this research, fluorescence imaging method was employed to observe the intracellular uptake of NPs. For this purpose, CF was used as a fluorescence probe which accumulates in the cytoplasm of the cells and DAPI was employed as a nuclear staining agent. According to Fig. 7A, a very slight fluorescence was observed at 4 and 24 h after incubation with free CF in the cancer cells. By contrast, CF loaded NPs were quickly accumulated in the cytoplasmic of cancer cells after 4 h incubation which can be visualized by the bright green fluorescence (Fig. 7B). Furthermore, CF loaded PHBV/PLGA NPs exhibited remarkably higher fluorescence intensity in cancer cells after 24 h. These findings indicated the faster internalization of CF loaded NPs in the cancer cells. In addition, these results displayed that the cellular uptake of the NPs became more significant with increasing the cell culture time. The selection of CF as the stain was due to its hydrophilicity which is similar to the nature of 5FU and OXA. Low intracellular uptake of hydrophilic drugs remains as a problem. NPs as drug delivery systems can improve the cellular uptake of hydrophilic drugs [51]. Our findings are consistent with earlier findings by Sadhukha and Prabha that indicated internalization of carboplatin (a hydrophilic drug with poor uptake) entrapment in PLGA NPs was more than free carboplatin [51]. A significant factor that contributes to the anticancer drugs in the treatment of cancer is cellular uptake [52]. It is established that cellular uptake of NPs by the cancer cells is more via endocytosis rather than passive diffusion [34,53]. The change in the uptake pathway from diffusion to endocytosis (particularly for hydrophilic drugs) may be an important characteristic of the NPs which increases their cytotoxicity [34]. According to the results of previous studies, PHBV and PLGA NPs are taken up by endocytosis pathway in the cancer cells [17,54]. The proposed mechanism of endocytosis uptake of NPs is shown schematically in Fig. 8.

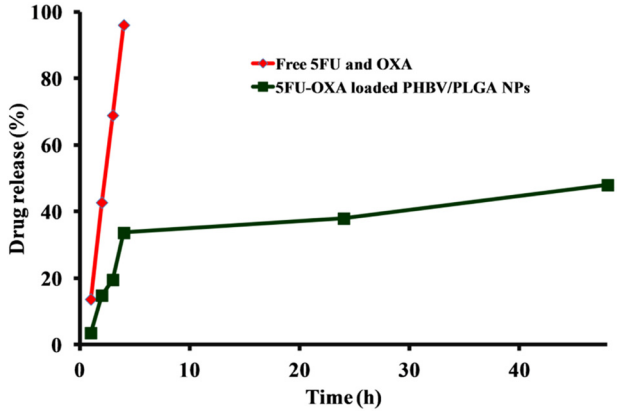

Fig. 6. In vitro release profile of free 5FU and OXA and 5FU-OXA loaded NPs.

3.7. Cytotoxicity assay

In vitro cytotoxic effect of free 5FU and OXA and 5FU-OXA loaded NPs on HT-29 and CT26 cells are shown in Fig. 9. All formulations showed dose-dependent cell proliferation inhibition behavior. IC_{50} values of free 5FU and OXA and 5FU-OXA loaded NPs on cancer cells are presented in Table 7. As illustrated in Fig. 8, in HT-29 and CT26 cells, a remarkable difference was observed between free 5FU and OXA and 5FU-OXA loaded NPs. Co-loaded NPs exhibited lower cell viabilities than mixture of the free drugs, suggesting the superiority of co-loaded NPs ($p < 0.05$). These results might be attributed to the different cell uptake pathways of free drugs and drug-loaded NPs [55]. As previously mentioned, endocytosis has been widely considered as main cellular uptake pathway for NPs in cancer cells [52]. Therefore, the more effectiveness of drugs loaded NPs is related to effective endocytosis of the NPs in the cells and more internalization of drugs in the cancer cells [51,56]. However, free 5FU and OXA absorb weakly and wash out rapidly owing to their hydrophilic nature [57]. In addition, the increase in the uptake of the drugs using PHBV/PLGA NPs led to reducing of IC_{50} value in comparison with that of free drugs. Similar results were

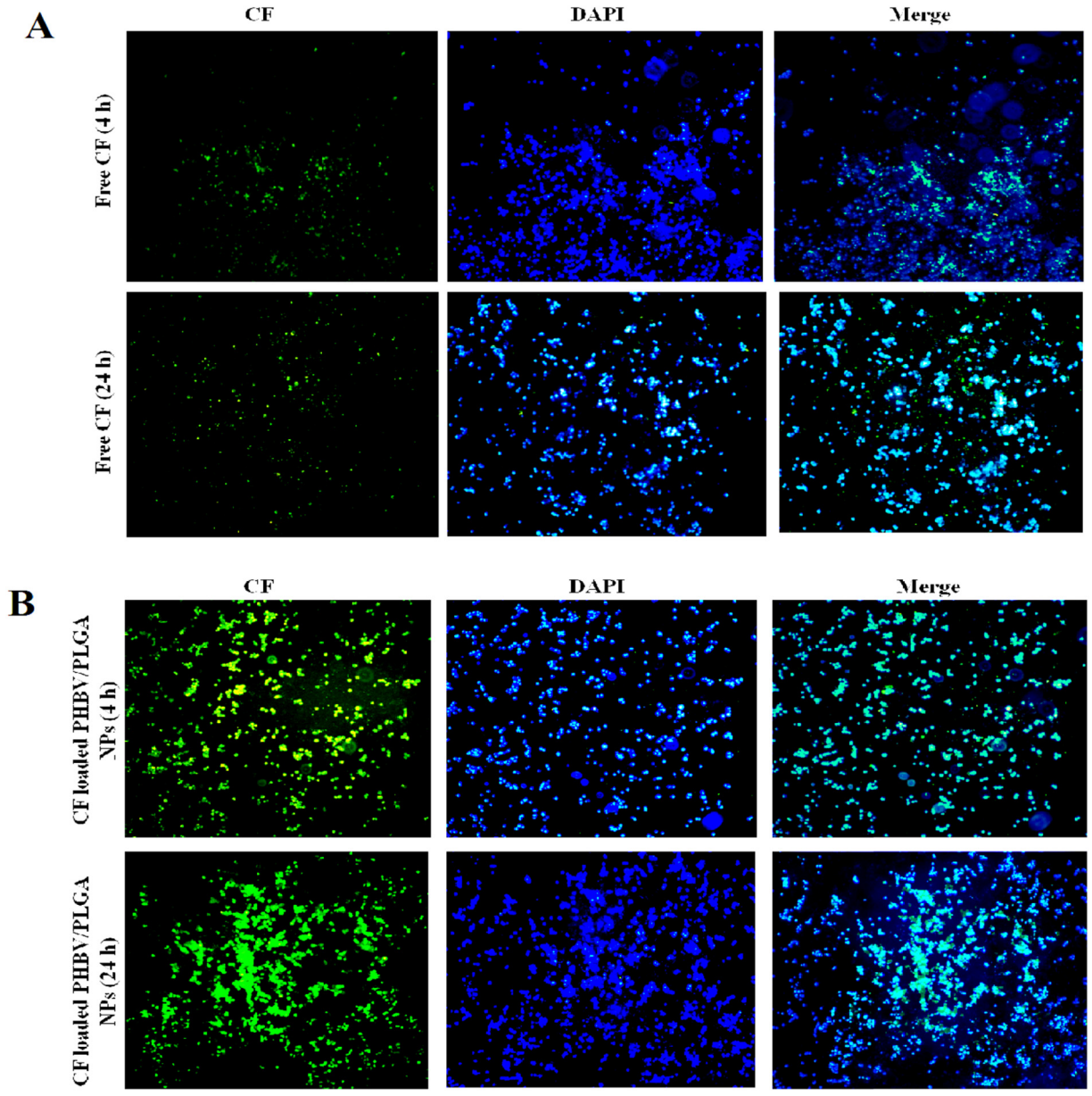

Fig. 7. Intracellular localization of A) free CF and B) CF loaded PHBV/PLGA NPs after 4 and 24 h.

reported by El-Hammadi et al. and Nair et al. that indicated 5FU loaded PLGA NPs exhibited anti-proliferative effect more than free 5FU in cancer cells and significantly reduced the IC_{50} of the drug [1,7]. Moreover, our findings are in-line with Vardhan et al. results which reported that cytotoxic effect of docetaxel containing PHBV NPs was much higher than the free docetaxel [20]. Masood et al. observed that ellipticine loaded PHBV NPs showed better cytotoxicity than the free drug. They also indicated that the delivery of the drug to cancer cells was mediated by water penetration and formation of pores in the PHBV polymeric core [58,59]. In the cancer therapy, the aim of employing drug delivery systems is to decrease the dose of drugs and as a result reducing side effects [59]. In addition, co-delivery of chemotherapy agents by NPs overcomes multi-drug resistance (MDR) and enhances drug concentration at tumor cells through improving their permeability [28]. The obtained results confirm that PHBV/PLGA NPs can present a novel prospect for colon cancer therapy with reducing adverse effect.

3.8. ROS generation assay

Previous studies have reported that 5FU and OXA exhibit their cytotoxic activity by generating of intracellular ROS [8,60]. ROS is an important regulator of cell apoptosis in cancer cells [61]. In order to investigate whether 5FU-OXA loaded PHBV/PLGA NPs could trigger ROS-mediated apoptosis, DCF was employed to determine intracellular ROS level. As shown in Fig. 10A, the co-delivery of 5FU and OXA in the NPs triggered significantly more ROS production compared to the free drugs in the cancer cells ($p < 0.05$). A significant increase of ROS levels was also observed in cancer cells after 48 h incubation, confirming that more drugs were internalized into the cells and induced higher ROS generation. The higher ROS production of 5FU-OXA loaded NPs displayed their efficiency towards anticancer potential. The present findings confirm the results of Jin et al. who reported that NPs induced ROS production and resulted apoptosis pathway in cancer cells. In order to examine the role of ROS contribution with NPs in inducing apoptosis, these researches

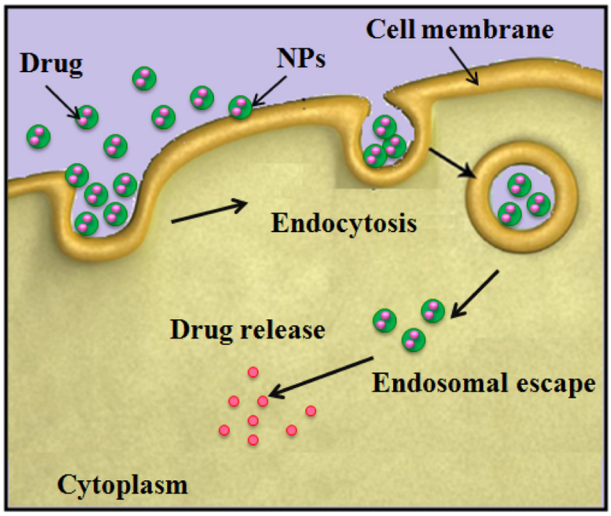

Fig. 8. Schematic illustration for endocytosis uptake of NPs.

co-cultured cancer cells with NPs and *N*-acetyl-L-cysteine (as a ROS inhibitor). They found that *N*-acetyl-L-cysteine considerably reduced the ability of NPs to inhibit cancer cells [62]. Our findings also agree with the results of Li et al. which found that co-delivery of paclitaxel and tetrandrine in NPs induced more ROS production in the cells compared to free drugs ($p < 0.05$) [63]. According to these findings, it seems that the production of ROS is an important mechanism that might contribute to the cytotoxicity of 5FU-OXA loaded NPs in the cancer cells.

3.9. Apoptosis study

Since generations of ROS by cells is considered as a signal of apoptotic, we have performed DAPI staining in HT-29 cells treated with the free 5FU and OXA, 5FU-OXA loaded NPs and compared to that of control group (untreated cells). As shown in Fig. 10B, 5FU-OXA loaded NPs induced significantly more apoptosis than free drugs; while, no apoptosis was observed in the control group. Nuclear morphology analysis showed characteristic apoptotic changes including nuclear fragmentation, chromatin condensation and formation of apoptotic bodies in the cancer cells. However, the untreated cells exhibited normal nuclei. These results clearly indicate that 5FU-OXA loaded NPs could induce cell death in cancer cells through ROS-mediated apoptotic. It is worth noting that in comparison with free 5FU and OXA, 5FU-OXA loaded NPs represented more apoptosis with lower IC_{50} (35.48 μM compared to 72.44 μM). The better efficacy of 5FU-OXA loaded NPs in comparison to free drugs may be due to differential cellular uptake which increases their efficacy to induce apoptosis in cancer cells. As mentioned in

Table 7
IC_{50} values (μM) for free 5FU and OXA and 5FU-OXA loaded PHBV/PLGA NPs on cancer cells.

Formulation	HT-29	CT26
Free 5FU and OXA	72.44	45.71
5FU-OXA loaded PHBV/PLGA NPs	35.48	26.91

Section 3.5, the alteration in the uptake pathway of NPs from diffusion to endocytosis may lead to an increase in their cytotoxicity [34]. Apoptosis is considered as an ideal way to induce cell death in cancer cells [64]. In cancer, the therapeutic goal is to trigger apoptotic pathway rather than necrosis pathway. Because necrosis induces inflammation which results in further tissue damaging [65]. The mechanisms of apoptosis are highly complex. It has been reported that ROS overproduction leads to collapse of mitochondrial membrane potential [52]. This disruption results to the release of cytochrome *c* from mitochondria to cytosol which is a main initiator for triggering apoptosis pathway [66]. In cytoplasm the cytochrome *c* activates caspases which are an important regulator of apoptosis [37,67]. Our finding is similar with Zhang et al. results which reported that co-delivery of paclitaxel and tetrandrine in NPs triggered significantly more ROS production and promoted apoptosis in cancer cells [68]. In addition, Li et al. expressed that paclitaxel loaded NPs enhanced cytotoxic effects on cancer cells through ROS-mediated apoptotic [67].

3.10. Hemolysis assay

In vitro hemolysis assay was performed to evaluate whether PHBV/PLGA NPs are safe for intravenous injection. As shown in Fig. 11A, NPs exhibited no significant hemolytic activity at different concentrations (below 5.0%), which is confirming excellent safety for intravenous injection. Usually, a hemolysis of <5% is considered as safe [69]. The RBCs exposed to PBS (as negative control) and Triton X-100 (as positive control) exhibited a non-significant and significant hemolysis, respectively (Fig. 11B). These data confirm previous researches which reported that PHBV polymer is hemocompatible. Mendes et al. indicated that PHPV microparticles were hemocompatibile with RBCs [70]. Vardhan et al. observed that PHBV NPs had no cytotoxic effect on RBCs, suggesting their high hemocompatibility [20]. Moreover, Yadav et al. found that PLGA NPs did not exhibit hemolytic properties on RBCs [18].

3.11. In vivo anticancer activity and histopathological study

The experimental design for evaluation of anticancer activity of free 5FU and OXA and co-loaded in NPs in mice is schematically represented in Fig. 12A. According to Fig. 12B, compared with the rapid tumor growth of control groups, all formulations exhibited high efficacy in

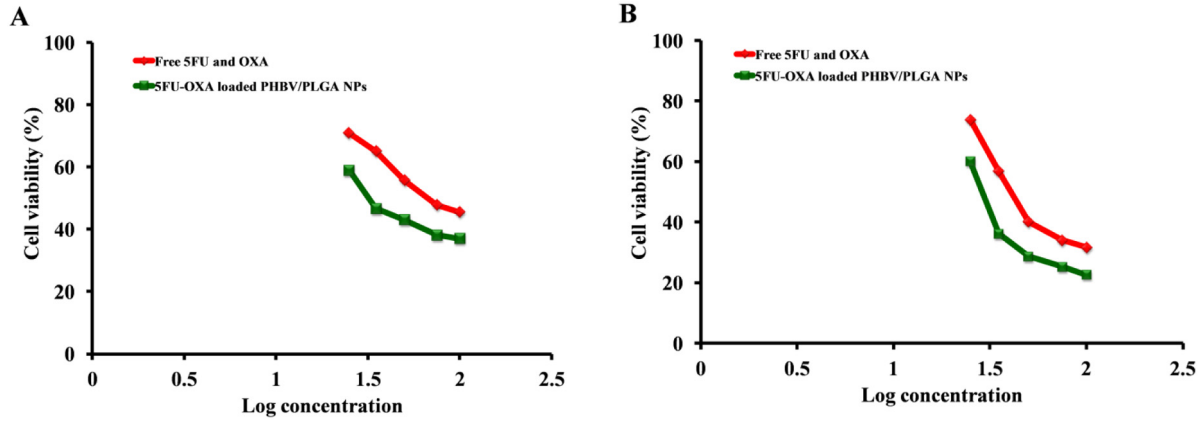

Fig. 9. In vitro cytotoxicity of free 5FU and OXA and 5FU-OXA loaded PHBV/PLGA NPs on A) HT-29 and B) CT26 cancer cells.

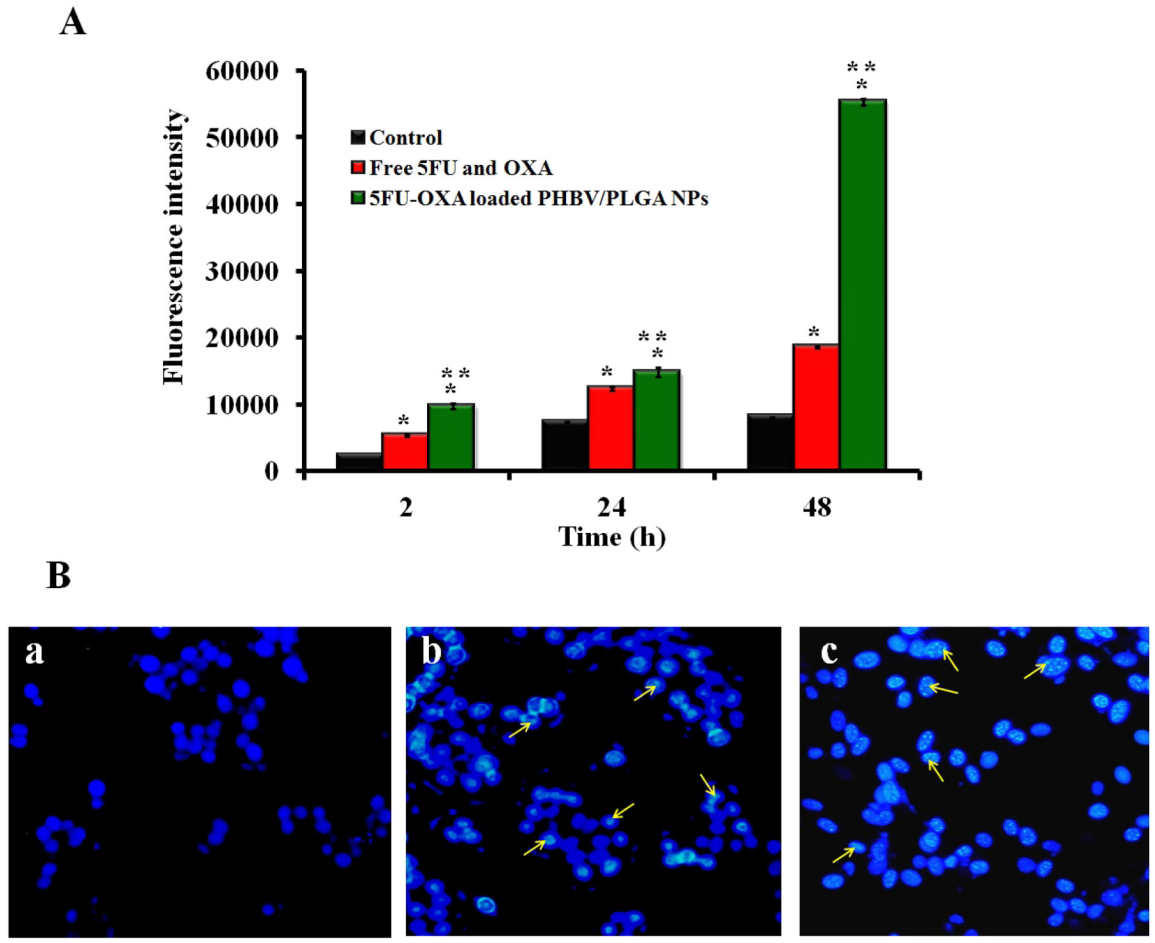

Fig. 10. A) Effect of free 5FU and OXA and 5FU-OXA loaded PHBV/PLGA NPs on generation of ROS in HT-29 cells and B) nuclear morphologic changes of HT-29 cells after 48 h treatment: (a) untreated cells (as control), (b) free 5FU and OXA and (c) 5FU-OXA loaded PHBV/PLGA NPs.

inhibiting the tumor growth. However, 5FU-OXA loaded NPs showed better antitumor effect compared with the free drugs ($p < 0.05$). As illustrated in Fig. 12C, it can be obviously observed that tumor size of treated group with co-loaded NPs is smallest among treatment groups which confirm the potential of NPs system in the effective therapy of cancer. These findings support our in vitro cytotoxicity study, indicating that 5FU-OXA loaded NPs induced higher antitumor activity both in vitro and in vivo. As can be seen in Fig. 12D, the 5FU-OXA loaded NPs treated group exhibited lowest tumor cell density in tumor tissue between the groups; confirming tumor cell proliferation had been inhibited effectively in the 5FU-OXA loaded NPs treated group. In addition, no significant change was observed in the feeding, body weight and movement between the treated and the control groups (data not shown). The obtained results further confirmed our hypothesis that co-loaded NPs can be successfully employed for treatment of colon cancer with great clinical application prospects. The superior antitumor activity of 5FU-

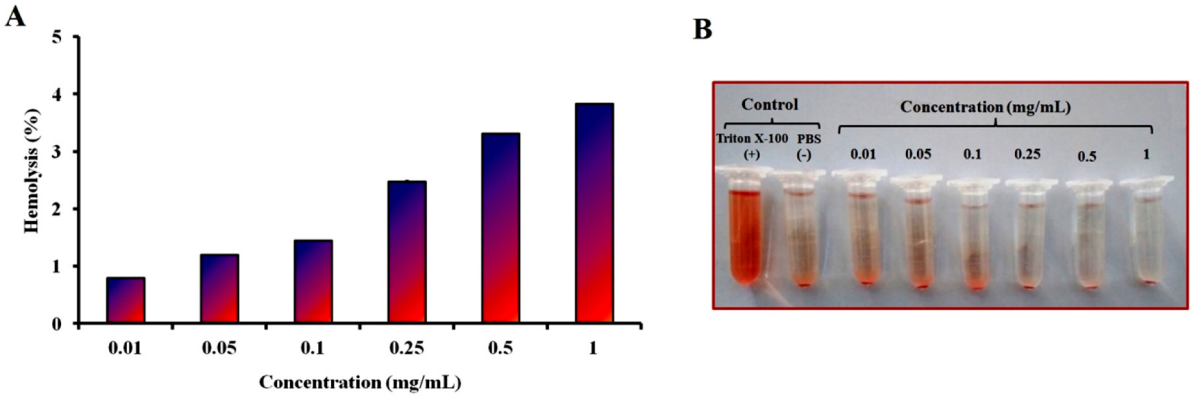

Fig. 11. Hemolysis assay: A) hemolysis (%) and B) image of RBCs treated with Triton X-100 (+), PBS (−) and different concentrations of PHBV/PLGA NPs.

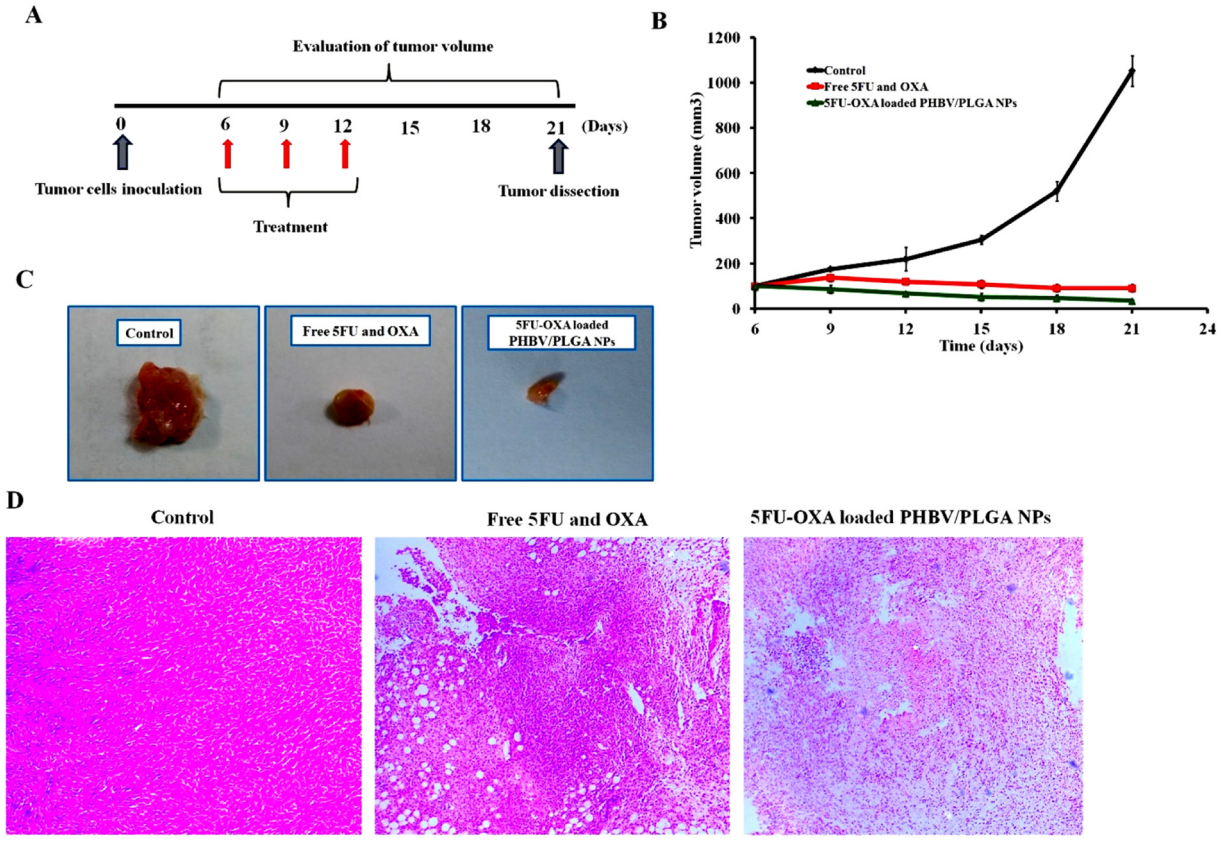

Fig. 12. Evaluation of in vivo anticancer activity of free 5FU and OXA and 5FU-OXA loaded PHBV/PLGA NPs: A) schematic representation of the experimental design, B) tumor volume, C) images of solid tumor and D) histopathology images of tumor sections with H&E staining of different experimental groups.

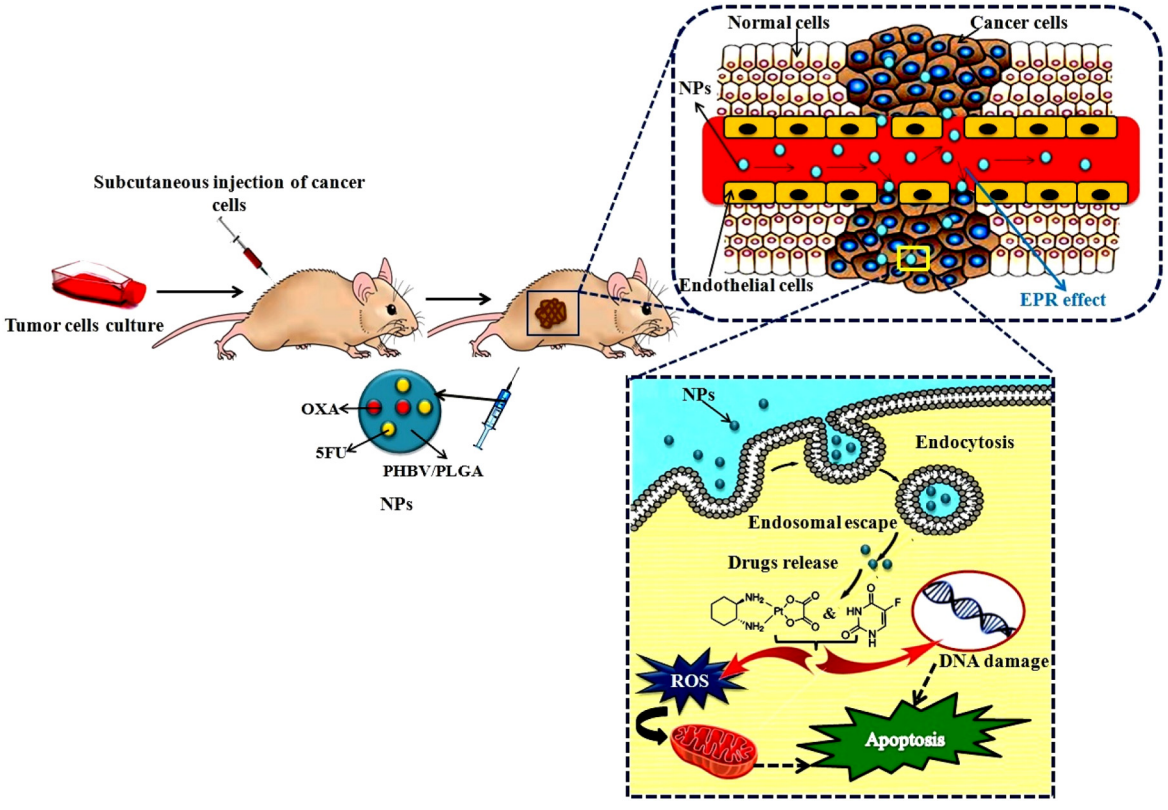

Fig. 13. Schematic representation of antitumor activity of 5FU-OXA loaded PHBV/PLGA NPs in cancer cells.

OXA loaded NPs may be attributed to coinstantaneous delivery of two drugs to the cancer cells and the efficient cellular uptake in the tumor tissues. NPs can be accumulated in the tumor tissues owing to impaired lymphatic drainage and leaky vasculature of tumors which is recognized as enhanced permeation and retention (EPR) effect. EPR effect facilitates permeation of NPs with size of 10–220 nm in the tumor tissues [14,43]. In the present research, NPs revealed size about 92.8 nm, which may effectively target cancer cells due to the EPR effect. These results are consistent with earlier findings by Zhu et al. They reported that doxorubicin and paclitaxel co-loaded NPs with nano-scaled size more effectively internalized into cancer cells due to EPR effect [71]. Zhang et al. also indicated that the superior antitumor effect of doxorubicin and curcumin co-loaded NPs might be associated to the sufficient cellular uptake and EPR effect [72]. On the other hand, according to the results of in vitro cytotoxic study that 5FU-OXA loaded NPs could induce apoptosis through production of ROS in cancer cells, it can be concluded that 5FU-OXA loaded NPs may induce apoptosis pathway in vivo and improve the antitumor efficacy of 5FU and OXA. Considering these results, it seems that better anticancer activity of 5FU-OXA loaded NPs may be related to the EPR effect and induction apoptosis pathway. The proposed mechanism of antitumor activity of 5FU-OXA loaded PHBV/PLGA NPs in cancer cells is presented schematically in Fig. 13.

4. Conclusion

In the study, PHBV/PLGA NPs were developed for delivery of 5FU and OXA in order to enhance anticancer efficacy. 5FU-OXA loaded PHBV/PLGA NPs showed higher cytotoxicity than free drugs and significantly induced ROS-dependent apoptotic pathway in cancer cells. Hemolysis assay indicated that NPs had good hemocompatibility, confirming they are suitable for IV administration. Moreover, co-loaded NPs presented superior antitumor activity. The present findings revealed that the co-delivery of PHBV/PLGA NPs provide a promising platform as a combination therapy in colon cancer treatment.

Conflicts of interest

There are no conflicts of interest.

Acknowledgment

The work was financially supported by Nanotechnology Research Center, Ahvaz Jundishapur University of Medical Sciences, Ahvaz, Iran (grant No. 111).

References

[1] K.L. Nair, S. Jagadeeshan, S.A. Nair, G.S. Kumar, Int. J. Nanomedicine 6 (2011) 1685–1697.
[2] P.A. McCarron, A.D. Woolfson, S.M. Keating, J. Pharm. Pharmacol. 52 (2000) 1451–1459.
[3] R. Seda, M. Pulat, J. Nanomater. (2012) 1–10.
[4] Y. Li, S. Duan, H. Jia, C. Bai, L. Zhang, Z. Wang, Acta Biochim. Biophys. Sin. 46 (2014) 460–470.
[5] S. Tummala, G. Kuppusamy, M.N. Satish Kumar, T.K. Praveen, A. Wadhwani, Drug Deliv. 23 (2016) 2902–2910.
[6] Y.S. Krishnaiah, V. Satyanarayana, B. Dinesh Kumar, R.S. Karthikeyan, P. Bhaskar, Eur. J. Pharm. Sci. 19 (2003) 355–362.
[7] M.M. El-Hammadi, A.V. Delgado, C. Melguizo, J.C. Prados, J.L. Arias, Int. J. Pharm. 516 (2017) 61–70.
[8] M.P. Liu, M. Liao, C. Dai, J.F. Chen, C.J. Yang, M. Liu, Z.G. Chen, M.C. Yao, Sci. Rep. 6 (2016) 34245.
[9] S. Tummala, K. Gowthamarajan, M.N. Satish Kumar, A. Wadhwani, Drug Deliv. 23 (2016) 1773–1787.
[10] K.A. Griffith, S. Zhu, M. Johantgen, M.D. Kessler, C. Renn, A.S. Beutler, R. Kanwar, N. Ambulos, G. Cavaletti, J. Bruna, C. Briani, A.A. Argyriou, H.P. Kalofonos, L.M. Yerges-Armstrong, S.G. Dorsey, J. Pain Symptom Manag. 54 (2017) 701–706.e701.
[11] O.M. Alian, A.S. Azmi, R.M. Mohammad, Clin. Transl. Med. 1 (2012) 26.
[12] S. Tummala, M.N. Kumar, S.K. Pindiprolu, Drug Deliv. 23 (2016) 3505–3519.
[13] H. Song, H. Xiao, M. Zheng, R. Qi, L. Yan, X. Jing, J. Mater. Chem. B 2 (2014) 6560–6570.
[14] B. Bahrami, M. Hojjat-Farsangi, H. Mohammadi, E. Anvari, G. Ghalamfarsa, M. Yousefi, F. Jadidi-Niaragh, Immunol. Lett. 190 (2017) 64–83.
[15] S.M. Masloub, M.H. Elmalahy, D. Sabry, W.S. Mohamed, S.H. Ahmed, Arch. Oral Biol. 64 (2016) 1–10.
[16] Z. Hafezi Ghahestani, F. Alebooye Langroodi, A. Mokhtarzadeh, M. Ramezani, M. Hashemi, Artif. Cells Nanomed. Biotechnol. 45 (2017) 955–960.
[17] S. Acharya, S.K. Sahoo, Adv. Drug Deliv. Rev. 63 (2011) 170–183.
[18] A.K. Yadav, A. Agarwal, G. Rai, P. Mishra, S. Jain, A.K. Mishra, H. Agrawal, G.P. Agrawal, Drug Deliv. 17 (2010) 561–572.
[19] E. Moghimipour, Z. Ramezani, S. Handali, Curr. Drug Deliv. 10 (2013) 151–157.
[20] H. Vardhan, P. Mittal, S.K.R. Adena, M. Upadhyay, B. Mishra, Int. J. Biol. Macromol. 103 (2017) 791–801.
[21] A. Banerjee, S. Pathak, V.D. Subramanium, D. G, R. Murugesan, R.S. Verma, Drug Discov. Today 22 (8) (2017) 1224–1232.
[22] F. Masood, Mater. Sci. Eng. C 60 (2016) 569–578.
[23] C. Peptu, M. Kowalczuk, 8 - Biomass-derived polyhydroxyalkanoates: biomedical applications, in: V. Popa, I. Volf (Eds.), Biomass as Renewable Raw Material to Obtain Bioproducts of High-Tech Value, Elsevier 2018, pp. 271–313.
[24] M. Koller, Molecules 23 (2018) 362, https://doi.org/10.3390/molecules23020362 Basel, Switzerland.
[25] A. Pich, N. Schiemenz, C. Corten, H.-J.P. Adler, Polymer 47 (2006) 1912–1920.
[26] E. Ten, L. Jiang, M.P. Wolcott, Carbohydr. Polym. 90 (2012) 541–550.
[27] W. Li, Z. Jan, Y. Ding, Y. Liu, C. Janko, M. Pischetsrieder, C. Alexiou, A.R. Boccaccini, Sci. Rep. 6 (2016) 23140.
[28] M. Afsharzadeh, M. Hashemi, A. Mokhtarzadeh, K. Abnous, M. Ramezani, Artif. Cells Nanomed. Biotechnol. (2017) 1–16.
[29] X.H. Zhu, C.H. Wang, Y.W. Tong, J. Biomed. Mater. Res. A 89 (2009) 411–423.
[30] J.U.N. Guo, S.-H. Wu, W.-G. Ren, X.-L. Wang, A.-Q. Yang, Exp. Ther. Med. 10 (2015) 2305–2310.
[31] Q. Lin, Y. Cai, M. Yuan, L. Ma, M. Qiu, J. Su, Oncol. Rep. 32 (2014) 2405–2410.
[32] J.Q. Li, S.L. Wang, F. Xu, Z.Y. Liu, R. Li, Anti-Cancer Drugs 21 (2010) 600–608.
[33] C. Nguyen, J.M. Christensen, T. Nguyen, Pharmacol. Pharm. 5 (2014) 620–635.
[34] X. Zhao, K. Yang, R. Zhao, T. Ji, X. Wang, X. Yang, Y. Zhang, K. Cheng, S. Liu, J. Hao, H. Ren, K.W. Leong, G. Nie, Biomaterials 102 (2016) 187–197.
[35] R. Bharti, G. Dey, I. Banerjee, K.K. Dey, S. Parida, B.N. Kumar, C.K. Das, I. Pal, M. Mukherjee, M. Misra, A.K. Pradhan, L. Emdad, S.K. Das, P.B. Fisher, M. Mandal, Cancer Lett. 388 (2017) 292–302.
[36] A. Avalos, A.I. Haza, D. Mateo, P. Morales, J. Appl. Toxicol. 34 (2014) 413–423.
[37] R. Vivek, R. Thangam, V. Nipunbabu, T. Ponraj, S. Kannan, Int. J. Biol. Macromol. 65 (2014) 289–297.
[38] B. Zhang, T. Wang, S. Yang, Y. Xiao, Y. Song, N. Zhang, S. Garg, J. Control. Release 238 (2016) 10–21.
[39] Y. Jin, X. Ren, W. Wang, L. Ke, E. Ning, L. Du, J. Bradshaw, Int. J. Pharm. 420 (2011) 378–384.
[40] T.A. Wani, A. Ahmad, S. Zargar, N.Y. Khalil, I.A. Darwish, Chem. Cent. J. 6 (2012) 134.
[41] T. Nahata, T.R. Saini, Drug Dev. Ind. Pharm. 34 (2008) 668–675.
[42] C. Zeng, W. Jiang, M. Tan, X. Yang, C. He, W. Huang, J. Xing, Eur. J. Pharm. Sci. 85 (2016) 123–131.
[43] H. Fasehee, R. Dinarvand, A. Ghavamzadeh, M. Esfandyari-Manesh, H. Moradian, S. Faghihi, S.H. Ghaffari, J. Nanobiotechnology 14 (2016) 32.
[44] P. Singh, G. Tyagi, R. Mehrotra, A.K. Bakhshi, Drug Test. Anal. 1 (2009) 240–244.
[45] J.S. Lee, G.S. Chae, T.K. An, G. Khang, S.H. Cho, H.B. Lee, Macromol. Res. 11 (2003) 183–188.
[46] M. Nasr, M.K. Ghorab, A. Abdelazem, Acta Pharm. Sin. B 5 (2015) 79–88.
[47] D. Zhang, J. Zhang, K. Jiang, K. Li, Y. Cong, S. Pu, Y. Jin, J. Lin, Spectrochim. Acta A Mol. Biomol. Spectrosc. 152 (2016) 501–508.
[48] I. Amjadi, M. Rabiee, M.-S. Hosseini, Iranian J. Pharm. Res. 12 (2013) 623–634.
[49] S. Manoochehri, B. Darvishi, G. Kamalinia, M. Amini, M. Fallah, S.N. Ostad, F. Atyabi, R. Dinarvand, Daru 21 (2013) 58.
[50] M. Kouhi, M.P. Prabhakaran, M. Shamanian, M. Fathi, M. Morshed, S. Ramakrishna, Compos. Sci. Technol. 121 (2015) 115–122.
[51] T. Sadhukha, S. Prabha, AAPS PharmSciTech 15 (2014) 1029–1038.
[52] L. He, H. Lai, T. Chen, Biomaterials 51 (2015) 30–42.
[53] R.H. Gaonkar, S. Ganguly, S. Dewanjee, S. Sinha, A. Gupta, S. Ganguly, D. Chattopadhyay, M. Chatterjee Debnath, Sci. Rep. 7 (2017) 530.
[54] J.P. Penaloza, V. Marquez-Miranda, M. Cabana-Brunod, R. Reyes-Ramirez, F.M. Llancalahuen, C. Vilos, F. Maldonado-Biermann, L.A. Velasquez, J.A. Fuentes, F.D. Gonzalez-Nilo, M. Rodriguez-Diaz, C. Otero, J. Nanobiotechnology 15 (2017) 1.
[55] S. Lv, Z. Tang, M. Li, J. Lin, W. Song, H. Liu, Y. Huang, Y. Zhang, X. Chen, Biomaterials 35 (2014) 6118–6129.
[56] S. Dadashzadeh, F.H. Derakhshandeh, K. Fau-Shirazi, F.H. Shirazi, 9-nitrocamptothecin polymeric nanoparticles: cytotoxicity and pharmacokinetic studies of lactone and total forms of drug in rats, Anticancer Drugs 19 (8) (2008) 805–811.
[57] A.C. Mattos, C. Altmeyer, T.T. Tominaga, N.M. Khalil, R.M. Mainardes, Eur. J. Pharm. Sci. 84 (2016) 83–91.
[58] F. Masood, P. Chen, T. Yasin, N. Fatima, F. Hasan, A. Hameed, Mater. Sci. Eng. C Mater. Biol. Appl. 33 (2013) 1054–1060.
[59] E. Locatelli, M. Comes Franchini, J. Nanopart. Res. 14 (2012) 1316.
[60] V. Santoro, R. Jia, H. Thompson, A. Nijhuis, R. Jeffery, K. Kiakos, A.R. Silver, J.A. Hartley, D. Hochhauser, J. Natl. Cancer Inst. 108 (2016), djv394. .
[61] R.D. Dubey, A. Saneja, A. Qayum, A. Singh, G. Mahajan, G. Chashoo, A. Kumar, S.S. Andotra, S.K. Singh, G. Singh, S. Koul, D.M. Mondhe, P.N. Gupta, RSC Adv. 6 (2016) 74586–74597.
[62] H. Jin, J. Pi, F. Yang, J. Jiang, X. Wang, H. Bai, M. Shao, L. Huang, H. Zhu, P. Yang, L. Li, T. Li, J. Cai, Z.W. Chen, Sci. Rep. 6 (2016) 30782.

[63] X. Li, X. Lu, H. Xu, Z. Zhu, H. Yin, X. Qian, R. Li, X. Jiang, B. Liu, Mol. Pharm. 9 (2012) 222–229.
[64] J.J. Pillai, A.K.T. Thulasidasan, R.J. Anto, N.C. Devika, N. Ashwanikumar, G.S.V. Kumar, RSC Adv. 5 (2015) 25518–25524.
[65] P. Davidovich, C.J. Kearney, S.J. Martin, Biol. Chem. 395 (2014) 1163–1171.
[66] B. Shen, P.-J. He, C.-L. Shao, PLoS One 8 (2013), e84610. .
[67] Y. Li, M. Guo, Z. Lin, M. Zhao, M. Xiao, C. Wang, T. Xu, T. Chen, B. Zhu, Int. J. Nanomedicine 11 (2016) 6693–6702.
[68] J. Zhang, L. Wang, H. Fai Chan, W. Xie, S. Chen, C. He, Y. Wang, M. Chen, Sci. Rep. 7 (2017) 46057.
[69] S. Yang, B. Zhang, X. Gong, T. Wang, Y. Liu, N. Zhang, Int. J. Nanomedicine 11 (2016) 2329–2343.
[70] J.B. Mendes, M.K. Riekes, V.M. de Oliveira, M.D. Michel, H.K. Stulzer, N.M. Khalil, S.F. Zawadzki, R.M. Mainardes, P.V. Farago, Sci. World J. 2012 (2012) 542937.
[71] D. Zhu, S. Wu, C. Hu, Z. Chen, H. Wang, F. Fan, Y. Qin, C. Wang, H. Sun, X. Leng, D. Kong, L. Zhang, Acta Biomater.
[72] Y. Zhang, C. Yang, W. Wang, J. Liu, Q. Liu, F. Huang, L. Chu, H. Gao, C. Li, D. Kong, Q. Liu, J. Liu, Sci. Rep. 6 (2016) 21225.